PCCP

Cite this: *Phys. Chem. Chem. Phys.*, 2011, **13**, 14928–14936

www.rsc.org/pccp

PAPER

Self-doping of molecular quantum-dot cellular automata: mixed valence zwitterions

Yuhui Lu and Craig Lent*

Received 27th April 2011, Accepted 12th June 2011
DOI: 10.1039/c1cp21332f

Molecular quantum-dot cellular automata (QCA) is a promising paradigm for realizing molecular electronics. In molecular QCA, binary information is encoded in the distribution of intramolecular charge, and Coulomb interactions between neighboring molecules combine to create long-range correlations in charge distribution that can be exploited for signal transfer and computation. Appropriate mixed-valence species are promising candidates for single-molecule device operation. A complication arises because many mixed-valence compounds are ions and the associated counterions can potentially disrupt the correct flow of information through the circuit. We suggest a self-doping mechanism which incorporates the counterion covalently into the structure of a neutral molecular cell, thus producing a zwitterionic mixed-valence complex. The counterion is located at the geometrical center of the QCA molecule and bound to the working dots *via* covalent bonds, thus avoiding counterion effects that bias the system toward one binary information state or the other. We investigate the feasibility of using multiply charged anion (MCA) boron clusters, specifically *closo*-borate dianion, as building blocks. A first principle calculation shows that neutral, bistable, and switchable QCA molecules are possible. The self-doping mechanism is confirmed by molecular orbital analysis, which shows that MCA counterions can be stabilized by the electrostatic interaction between negatively charged counterions and positively charged working dots.

1. Introduction

The quantum-dot cellular automata (QCA)[1–8] approach is a promising paradigm for nanoelectronic binary computing. In the QCA scheme, binary information is represented by the charge configuration of QCA cells. As Fig. 1 shows schematically, each QCA cell contains four quantum dots, which are simply places at which electrons can be localized. Two mobile charges occupy antipodal sites of the cell, providing two charged configurations with which the binary information "0" and "1" can be encoded. The Coulomb interaction between neighboring cells provides device-device coupling for information transfer. This interaction is the basis of QCA device operation. Fig. 1(b) also shows a QCA wire[2] that can transfer a bit from one side to the other. More complicated device structure like a QCA inverter, fan-in, fan-out, majority logic gate, and full adder have been proposed[3] and demonstrated experimentally.[7,8]

QCA devices can be shrunk to the molecular level.[9–16] Each molecule acts as a QCA cell, and the redox centers of the molecule constitute the quantum dots, with tunneling paths provided by bridging ligands. Molecular QCA shares many of the advantages and disadvantages of other approaches to molecular electronics. Molecules can be synthesized in tremendous numbers with atomic-level precision and repeatability, and their small size conceivably could allow densities of 10^{11} to 10^{12} devices/cm^2 range.[17,18] This density and uniformity is far beyond what is practical *via* traditional device fabrication, though along with these advantages comes the extraordinary challenge of bottom-up assembly into large-scale, complex devices. The true advantage of molecular QCA is its greatly reduced heat dissipation, as computation proceeds from the rearrangement of charge, with no requirement for continuous current flow to transmit and process data. Additionally, because the amount of charge switched is constant in number of electrons, QCA devices inherently improve as size is reduced.

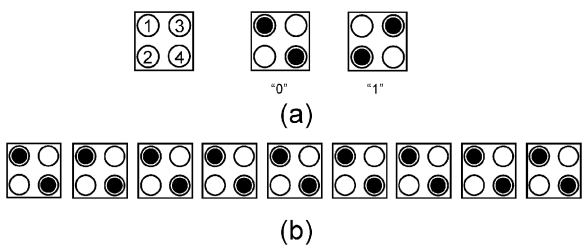

Fig. 1 (a) Schematic of a QCA cell. The four dots are labeled 1, 2, 3, and 4. Binary information is encoded in the charge configuration. (b) A QCA wire.

Department of Electrical Engineering, University of Notre Dame, Notre Dame, IN 46556, USA. E-mail: lent@nd.edu

The strong interaction between neighboring molecules provides sufficiently high coupling energy, so molecular QCA can operate at room temperature as shown previously.[13,14]

Several QCA candidate mixed-valence molecules have been synthesized and characterized by Fehlner and co-workers.[9–12] A double-dot molecule *trans*-$Ru(dppm)_2(C{\equiv}CFc)(NCCH_2CH_2NH_2)$ dication[9] has been attached to a Si substrate, and a measurement of capacitance between two redox centers showed the switchable bistable charge configuration which is a fundamental requirement for QCA operation. A more complicated four-dot molecule has also been synthesized and isolated.[10,11] Theoretical studies[14] of these molecules again show the requisite bistable charge configurations, and that the Coulomb interactions between neighboring molecules are sufficient to support bit transfer at room temperature. More recent scanning tunneling microscopy (STM) investigation demonstrated the charge localization of QCA candidate molecules.[19]

It is important to control the effect of counterions in the QCA arrays because in most cases, mixed-valence states are created by chemical oxidation/reduction, which inevitably introduces counterions in to maintain charge neutrality. The effect of counterions has been discussed in detail in the literature,[9,20] where the QCA cells were switched by the combined influence of external field and the movement of counterions.

2. Neutral QCA molecules

A natural way to eliminate counterion effects is to use *neutral* molecules with internal mobile charges as molecular QCA cells, that is, zwitterionic mixed-valence complexes. To this end, we examine incorporating a donor or acceptor within the molecule at an electrostatically symmetric position. This donor/acceptor provides the required mobile charge—electrons or holes. The donor/acceptor can be built into QCA molecules *via* covalent bonds. If the oxidation potential of the donor/acceptor is properly controlled, mobile charges can be generated in the working dots of the molecule. The donor/acceptor moiety will become charged, and that charge must not bias the molecular cell into either configuration (a logical "1" or "0"). In QCA operation, the logical state of the molecular cell should be determined by the state of its neighbors. This "self-doping" can be accomplished by choosing an appropriately symmetric position for the donor/acceptor dot.

A plausible scheme is suggested as shown in Fig. 2. Here an electron deficient dot is added in the center of the molecule, connecting to the four working dots *via* covalent bonds. If the oxidation potential of the acceptor site is properly designed, two working dots could be oxidized by the acceptor, creating two holes in the peripheral dots and two electrons in the center acceptor. These two electrons will be fixed in the center acceptor since it is electron deficient; the two holes, due to the Coulomb repulsion, will occupy two antipodal working dots.

The mobile holes can be arranged in either the "0" state or the "1" state as shown in the figure. In isolation, these two states have the same energy. The presence of another nearby molecule (or appropriate external driver) lifts this degeneracy so that either a "0" or "1" state is energetically preferred. The central dot is here playing the role of the counterion, providing

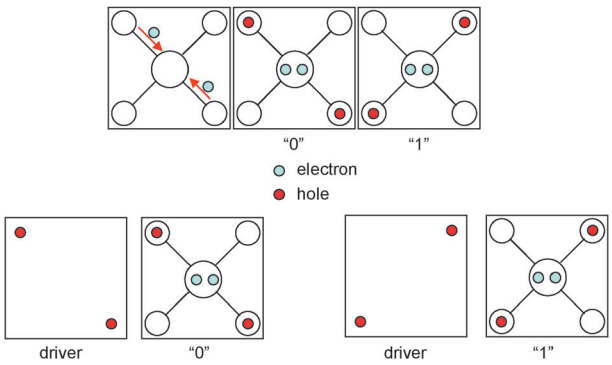

Fig. 2 The self-doping mechanism of a molecular QCA.

the neutralizing charge. But in this case, the counterion is in fact fixed at the geometrical center of the QCA cell and is part of the molecule itself. Its Coulombic effect is symmetric to the "0" and "1" states, so the state of a cell is decided by the state of its neighboring cells. The unwanted biasing effects of counterions are thereby eliminated.

To accomplish this "self-doping" using the approach shown in Fig. 2 requires a moiety in the cell center which is doubly charged. The recently-shown stability of gas-phase multiply charged anions (MCAs)[21–24] may provide an important element in creating neutral molecular QCA. The research field of MCAs in the gas phase received great impetus since the experimental observation of small MCAs in 1990.[25] A large number of experimental[26,27] and theoretical studies[21,22] have established the existence of MCAs in the gas phase. Kalcher and Sax have written a detailed review of MCAs.[24] Here we focus our interest on using the MCAs as building blocks of QCA cells.

Among different types of MCAs, boron clusters are of particular interest for the present purpose. Many boron clusters are electron deficient and contain three-dimensional cage structures. The elucidation of the chemical bonding in the boron clusters and the confirmation of their cage structures open opportunities to use them as new types of building blocks in chemistry. The *closo*-hexaborate dianion $B_6H_6^{2-}$ has a closed-shell electronic configuration and an octahedral cage structure, which make it an ideal linker group to connect the working dots of QCA cells. The closed-shell electron configuration is important because open-shell systems are generally too reactive and susceptible to cluster-cluster agglomeration. The octahedral cage structure makes it possible to bind four redox centers (working dots) to the linker, and the remaining axial boron atoms provide the degrees of freedom to build a leg or strut to attach the QCA cell on the surface of substrates, as shown in Fig. 3.

Recent studies have pointed out that, even though the *closo*-hexoborate dianion $B_6H_6^{2-}$ is not stable in the gas phase, some of its derivatives are. For example, $B_6L_6^{2-}$ and $B_6H_2L_4^{2-}$ (L = BO, CN or NC) are stable in the gas phase, according to the *ab initio* study of Zint *et al.*[22] The stability of these derivatives, as explained by these authors, comes from the extra molecular space provided by the diatomic pseudo-halogen ligands—the larger space allows the distribution of the extra electrons across a bigger volume, thus reducing the Coulomb repulsion significantly. We here consider the possibility

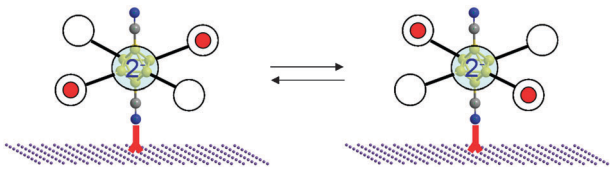

Fig. 3 The scheme of using a boron cluster as a "dopant."

of using derivatives of $B_6H_6^{2-}$ as the central acceptor of QCA cells.

We explore the feasibility of using the $B_6L_6^{2-}$ fragment as the built-in counterion of neutral QCA cells by employing a quantum chemistry *ab initio* technique. Our purpose is to investigate the interaction between this counterion and the working dots. We aim at understanding the electronic structure of QCA cells when certain working dots are bound to this built-in counterion. To this end, a proper working dot should be chosen carefully, such that the self-doping mechanism can create mobile charges in the QCA cell, as mentioned above. We use allyl groups to model working dots, connecting to the $B_6(CN)_2$ fragment through a C≡C triple bond. Though real working dots would no doubt be constructed differently (experimentally organometallic dots have been used,[9–12,19]) these allyl groups are useful because the QCA cell so constructed is amenable to high level *ab initio* calculations.[13,28] The purpose of using a C≡C triple bond binding an allyl group and the $B_6(CN)_2$ fragment is to maintain the D_{2h} symmetry of the QCA cell, which, again, simplifies our calculations.

The constructed model cell $B_6(CN)_2(C{\equiv}CC_3H_4)_4$ is shown in Fig. 4(a), hereafter denoted as molecule **1**. To identify the mechanism which stabilizes the zwitterionic configuration, we will systematically reduce the number of ligands and redox centers and examine the resulting $B_6H_2(C{\equiv}CC_3H_4)_4$, molecule **2**, $B_6H_4(C{\equiv}CC_3H_4)_2$, molecule **3**, and non-bonded supermolecular system $B_6H_6(C_3H_4)_2$, molecule **4**, with standard *ab initio* quantum chemical methods. Molecules **2**, **3**, and **4** are shown in Fig. 4(b)–(d). We focus on the electronic structure of these MCA-cation complexes and discuss the effects of the ligands and working dots on the geometric and electronic properties of the complexes. This paper is organized as follows: the computational details are given in Section 3. In Section 4, we present our results describing the electronic properties of **1**, **2**, **3**, and **4**. For molecule **1**, we also demonstrate the charge bistability and switching characteristics when driven by a point charge driver. Finally, a brief summary of our main results is given in Section 5.

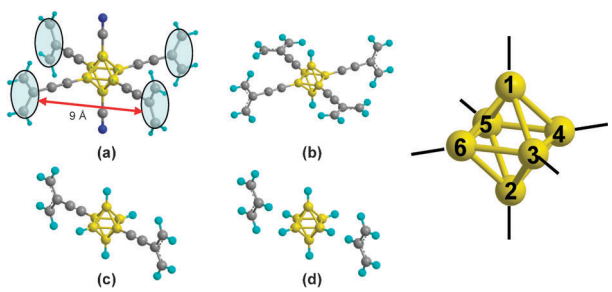

Fig. 4 The structure of the model molecules **1**, **2**, **3**, and **4**. Six boron atoms are labeled as 1 to 6. (a) Molecule **1**, $B_6(CN)_2(C{\equiv}CC_3H_4)_4$. A boron cluster is used as an integrated acceptor, and allyl groups as the active quantum dots. (b) Molecule **2**, $B_6H_2(C{\equiv}CC_3H_4)_4$. (c) Molecule **3**, $B_6H_4(C{\equiv}CC_3H_4)_2$. (d) Molecule **4**, $B_6H_6(C_3H_4)_2$.

3. Computational details

The calculation of **1**, **2**, **3**, and **4** includes geometry optimization and electronic structure. For **1**, we also study the bistablility of the charge configuration, a basic QCA requirement, and the switching between stable states induced by the Coulomb interaction with a neighboring molecule. The geometry optimizations within a given point group are carried out until the stationary points at the potential energy surface are found. For all stationary points, a harmonic vibrational analysis is implemented to identify the local minima on the PES, for which all frequencies possess only real values. The electronic stability of the central dot hexaborate dianion is investigated by calculating the binding energy of the excess electrons, which is quantified by the energy of the molecular orbitals that are occupied by the two doping electrons.

For molecule 1 and 2, there are four allyl groups each having one singly occupied π orbital. After "self-doping", two of those π orbitals become empty and the other two unpaired electrons remain on same orbitals. Therefore the neutral mixed-valence complexes 1 and 2 have biradical configurations. Computing the electronic structure of these molecules is challenging. It is well known that unrestricted Hartree–Fock based methods may suffer severely from spin contamination and the computational results often cannot be trusted. Density functional theory (DFT) generally suffers from spin contamination at a much less degree, but DFT has difficulty getting the charge localization correct.[16] In DFT calculations, the mobile electrons tend to delocalize over the donor and acceptor groups, and the donor–acceptor interactions are usually overestimated. The origin of this failure is attributable to the delocalization error of the exchange–correlation functional as well as the self-interaction error.[29] A multi-configurational self-consistent field (MCSCF) method is normally needed to obtain an accurate electronic structure of donor–acceptor electron transfer system. But a full MCSCF calculation is computationally intractable for systems we are considering here.

We employ restricted open-shell Hartree–Fock (ROHF) and restricted open-shell Møller–Plesset second-order perturbation (ROMP2) methods to avoid spin contamination. For a comparison, calculations are also conducted using the constrained density functional theory (CDFT). The CDFT method was first suggested by Dederich *et al.*[30] and more recently developed by Van Voorhis *et al.*[31–33] This method is based on the traditional density functional theory of Hohenberg, Kohn, and Sham,[34,35] but with the additional requirement that ground-state electron density satisfies some special constraint. When applied to mixed-valence complexes, this constraint requires the mobile electron localizing on either the donor site or the acceptor site, instead of delocalizing over both sites, as the traditional DFT method tends to do because of the self-interaction error.[29] CDFT has been successfully applied to study electron transfer in large molecular systems. We have also applied this method to calculate STM images of mixed-valence complexes.[19] The 6-31G* basis is used for all atoms.

ROHF and ROMP2 calculations have been done with the MOLPRO program,[36] and CDFT calculations have been conducted with the NWCHEM program.[37]

4. Results and discussion

4.1 $B_6(CN)_2(C{\equiv}CC_3H_4)_4$

The optimized geometry is displayed in Fig. 4(a), and selected optimized bond lengths are listed in Table 1. The optimizations are conducted with D_{2h} molecular symmetry. Bond lengths between axial B and equatorial B atoms are 1.710 and 1.735 Å, obtained at the ROHF level, which is in agreement with Zint *et al.*'s calculation of CN substituted species.[22] Four equatorial B atoms form a rhombus with a lateral length of 1.727 Å. The B1–B3 bond length is 0.25 Å longer than that of the B1–B4 (see Fig. 4 for the numbering of boron atoms). That is because the two cationic allyl groups are connected to B3 and B5, while the two ally groups connected to B4 and B6 are neutral. It is the electrostatic interaction between cationic allyl groups and the anionic borane cage that shrinks the B1–B3 and B1–B5 bond length, resulting in a D_{2h}, instead of D_{4h} symmetry. As to the substituted ligand CN, the B–C and C–N bond lengths are 1.556 Å and 1.141 Å, corresponding to the covalent single bond and triple bond, respectively. Comparing the different geometries obtained at the ROHF level and ROMP2 level, we can see that electron correlation has a small effect on the boron cage; only the intraligand bond lengths are clearly stretched. The elongation of terminal multiple bonds attached to the *closo*-boron cluster has been observed in the literature.[22]

Turning to the geometry of the allyl groups, we see that the four allyls are not identical, but have two different geometries corresponding to their charge state. The C–C bond lengths of all four allyl groups are almost identical. The clear difference is in the C–C–C bond angle. Two allyl groups occupying the antipodal sites have a value of 121.3°, corresponding to allyl radicals. The C–C–C bond angles of the other two allyl groups are 113.7°, which is in agreement with the bond angle of the allyl cation as shown by Avriam.[38]

CDFT calculations were conducted by forcing two positive unit charges localize on a pair of antipodal allyl groups. From Table 1 one can see CDFT results are consistent with those of ROHF and ROMP2. Bond lengths between axial B and equatorial B atoms are 1.720 and 1.738 Å according to CDFT optimization. B–C and C–N bond lengths are predicted to be 1.534 Å and 1.167 Å, respectively. C–C–C bond angle is 120.9° for neutral allyl groups and 117.6° for cationic allyl groups. It is worth noting that in our CDFT calculations the charge constrained conditions were only applied on two antipodal allyl groups so that mobile charges do not delocalize among all four allyl groups. The extra two electrons accumulating on the borate moiety were caused by the electron-deficiency of boron cluster, not parameterized constraint requirement.

Molecule **1** has two stable charge configurations, as demonstrated in Fig. 5, which shows the electrostatic isopotential surface. The charge distribution analysis shows that the central boron cluster group has two extra electrons, and two allyl groups are positively charged. These two positively charged groups, occupying antipodal positions, give two stable charge configurations which are energetically degenerate, so they can be used to represent binary information. The advantage is that the counterion is fixed at the geometrical center of the molecule, which does not influence the degeneracy of the "0" and "1" states.

More detailed molecular orbital analysis demonstrates that two unpaired allyl π electrons are indeed "doped" into the boron cluster. Fig. 6 shows the frontier orbitals of **1**. The HOMO − 3 and HOMO − 4 of **1** are singly occupied degenerate π orbitals that localize on two antipodal allyl groups. These two HOMOs are occupied by two unpaired electrons, which are information-bearing mobile electrons that can be switched to other two allyl groups. LUMO and LUMO + 1 are singly unoccupied degenerate π orbitals, localizing on the other two allyl groups. These two allyl orbitals become empty because two electrons transfer into the boron cluster, and occupy the b_{1g} orbital centered on the boron cluster. Comparing the frontier orbitals of **1** to the *closo*-hexaborate dianion $B_6H_6^{2-}$ (shown in Fig. 7), one can see that the triply degenerate t_{2g} and t_{1u} orbitals of $B_6H_6^{2-}$ evolve into the b_g and b_u orbitals of **1**. The HOMO orbital of **1**, which has b_{1g} symmetry, is equivalent to t_{2g} HOMO orbital of un-substituted $B_6H_6^{2-}$. The orbital analysis further confirms the self-doping mechanism: two energetically high-lying π electrons of the allyl groups can be trapped in the boron cluster to satisfy Wade's rule,[39] creating two holes inside the allyl groups. The configuration of these two holes can be used to encode binary information as discussed above.

Table 1 The optimized structural parameters (in Å) of $B_6(CN)_2(C{\equiv}CC_3H_4)_4$, $B_6H_2(C{\equiv}CC_3H_4)_4$, and $B_6H_4(C{\equiv}CC_3H_4)_2$ at ROHF, ROMP2, and constrained DFT/B3LYP levels. Boron atoms are numbered as shown in Fig. 4

		B_1–B_3	B_1–B_4	B_3–B_4	B–C	C–N	C–C–C	C–C–C(+)
$B_6(CN)_2(C{\equiv}CC_3H_4)_4$	ROHF	1.710	1.735	1.727	1.556	1.141	121.3	113.7
	ROMP2	1.714	1.741	1.729	1.531	1.188	121.9	112.1
	CDFT	1.720	1.738	1.734	1.534	1.167	120.9	117.6
$B_6H_2(C{\equiv}CC_3H_4)_4$	ROHF	1.724	1.748	1.713			120.7	113.0
	ROMP2	1.724	1.750	1.719			121.3	111.2
	CDFT	1.729	1.744	1.723			120.2	117.6
$B_6H_4(C{\equiv}CC_3H_4)_2$	ROHF	1.719	1.755	1.719				112.3
	ROMP2	1.720	1.752	1.720				110.5
	CDFT	1.724	1.746	1.724				117.5
$B_6(CN)_6^{2-a}$	HF	1.723	1.723	1.723	1.562	1.144		
	MP2	1.727	1.727	1.727	1.538	1.194		

[a] Results from ref. 22.

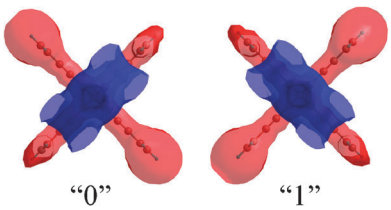

Fig. 5 Bistable charge configuration of molecule **1**, $B_6(CN)_2(C{\equiv}CC_3H_4)_4$. The bistability is shown by the electrostatic isopotential surface. The blue surface shows negative charge, and the red surface shows the positive charge (colors are displayed in the online version only). The *closo*-borate, locating at the geometrical center of 1, is negatively charged, while two peripheral allyl groups are positively charged. The different charge configurations are used to represent "0" and "1".

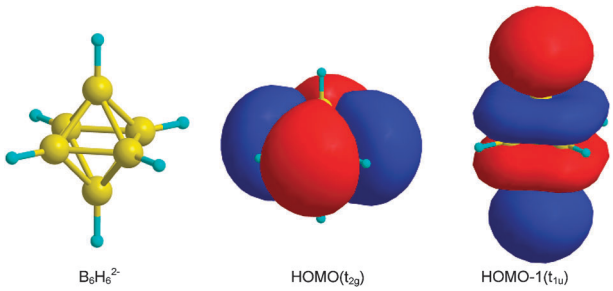

Fig. 7 HOMO and HOMO − 1 orbitals of the *closo*-hexaborate dianion $B_6H_6^{2-}$. The HOMO is triply degenerate t_{2g} orbitals and HOMO − 1 is triply degenerate t_{1u} orbitals. The extra two electrons are needed to stabilized the boron cluster according to the Wade's rule.

The coupling between neighboring QCA cells is characterized by the cell–cell response function, which is defined as one cell's polarization as a function of its neighboring cell's polarization.[1] For a four dot molecule like **1**, the QCA polarization of the molecule is proportional to its electric quadrupole moment. The cell–cell response function describes the switching behavior of one QCA cell under the Coulomb interaction of its neighboring cell. To calculate the cell–cell response function of 1, we employ a driver which consists of positive charges arranged on the corners of a square with a lateral length of 9 Å, mimicking the presence of a driver molecule, as shown in Fig. 8(a). The distance between the geometrical center of the point charge driver and that of molecule **1** is fixed at 18 Å, two times of the square lateral length. The magnitude of the positive driver charge on the four corners is varied smoothly to adjust the quadrupole moment of the driver Q_{driver}. The QCA response function of **1** under the Coulomb interaction of a neighboring molecule, shown in Fig. 8(b), is the induced molecular quadrupole moment as a function of the driver quadrupole moment. The molecular quadrupole moment is calculated for the case of frozen nuclear positions, for which the nuclear coordinates are intermediate between "0" state and "1" state. The intermediate structure is geometrically symmetrical, favoring neither "0" nor "1" state, and thus the calculated result can be explained by the electronic structure of the molecule, not by the effect of nuclear relaxation. In a previous study, it was found that the electron switch is caused mainly by the change of local field, with only a weak dependence on nuclear relaxation.[13] From Fig. 8(b) one can see that in the vicinity of zero polarization, a small input quadrupole moment induces a large quadrupole moment in the output, suggesting that a small change in the input charge configuration can switch a neighboring molecule from one state to the other. This provides the basis for QCA operation.

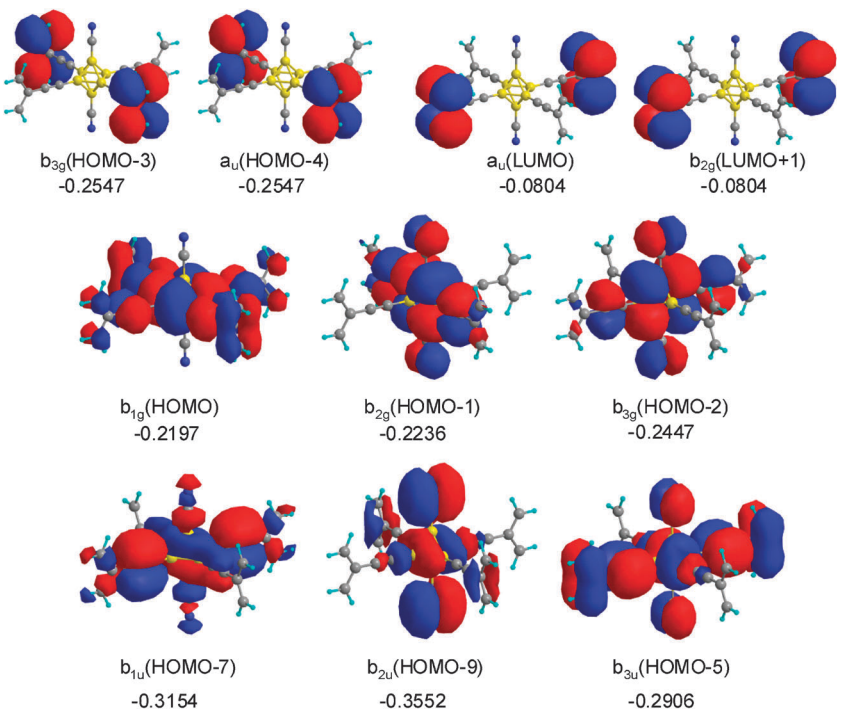

Fig. 6 Frontier molecular orbitals of molecule **1**, $B_6(CN)_2(C{\equiv}CC_3H_4)_4$. Orbital energies are given in Hartree, obtained from ROHF calculations.

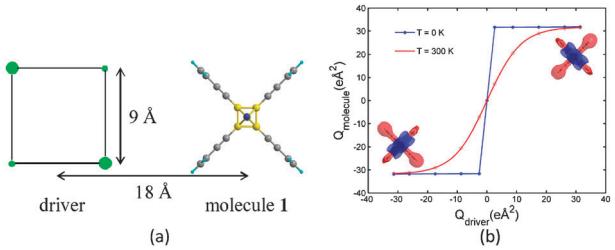

Fig. 8 (a) Geometry of the point charge quadrupole driver used as input to molecule **1**. The driver simulates the effect of another nearby molecular cell. (b) The response function of molecule **1** when driven by a neighboring molecule.

For molecule **1**, the Coulomb interaction tends to align neighboring molecules. Each molecular quadrupole moment induces the same quadrupole moment in its neighbor, at both 0 K and 300 K. The nonzero temperature response is calculated by taking the thermal expectation value of the molecular quadrupole moment calculated as follows:

$$Q(T) = (Q_0 + Q_1 e^{\frac{-(E_1-E_0)}{k_B T}})/(1 + e^{\frac{-(E_1-E_0)}{k_B T}}) \qquad (1)$$

in which T is the temperature, Q_0, Q_1, E_0 and E_1 are the quadrupole moment and total energy of the "0" and "1" states respectively, and k_B is Boltzman's constant. From Fig. 8 we can see that the quadrupole moment of two neighboring molecules tend to align. Even at room temperature, the Coulomb interaction is sufficient to switch neighboring molecules. Also, for Coulomb interactions between molecules, the built-in counterions have symmetric effects on the neighboring molecule, and so do not introduce a bias between the "0" and "1" states.

It worth noting that Fig. 8 demonstrates the response function of **1** obtained by the direct computing of the polarization and energy of two charge configurations. It does not address the dynamics or speed of switching, which would require the detailed study of the electron transfer matrix element, as shown in our previous work.[15] We note that comparable electron transfer in saturated borate zwitterions has been demonstrated by experiment.[40]

4.2 $B_6H_2(C{\equiv}CC_3H_4)_4$, $B_6H_4(C{\equiv}CC_3H_4)_2$, and $B_6H_6(C_3H_5)_2$

We turn to investigate the mechanism which stabilizes the dianion dopant inside these QCA molecules. In the above discussion we have considered the stable hexasubstituted $B_6(CN)_2(C{\equiv}CC_3H_4)_4$. We now reduce the number of ligands from six, to four, and then to two, and examine the resulting $B_6H_2(C{\equiv}CC_3H_4)_4$, $B_6H_4(C{\equiv}CC_3H_4)_2$, and $B_6H_6(C_3H_5)_2$ designated molecules **2**, **3**, and **4**, as shown in Fig. 4(b)–(d), in the same fashion. For all these species, we maintain D_{2h} symmetry for convenience in comparing the ligand influence on the frontier molecular orbitals, which are helpful in understanding the stability of the corresponding borate dopant.

Geometry optimization of molecule **2** reveals that the *closo*-borate is stretched along the four allyl groups, resulting in a longer boron–boron distance between axial and equatorial atoms than between axial and axial atoms (Table 1). The optimization shows that four allyl groups are divided into two groups. Two allyl groups are parallel to the B_4 equatorial plane, while the other two allyl groups are perpendicular to the B_4 equatorial plane. Like **1**, two mobile electrons localize in two antipodal allyl groups. The other two allyl π orbitals are empty orbitals LUMO and LUMO + 1 due to the "self-doping". The B6 cluster obtains two extra electrons to maintain a stable charge configuration. The Mulliken charge distribution analysis reveals that the charge density for each allyl group parallel to the B_4 equatorial plane is about +1, while allyl groups perpendicular to the B_4 equatorial plane are neutral. The charge distribution is consistent with the optimized geometry. The C–C–C bond angle of cationic allyl groups is 113°, compared with that of the neutral allyl groups, which is 120.7° (see Table 1). Again, ROHF, ROMP2, and CDFT calculations predict similar results on molecule **2**.

Further reduction of the number of ligands leads to the disubstituted $B_6H_4(C{\equiv}CC_3H_4)_2$ and non-substituted $B_6H_6(C_3H_5)_2$

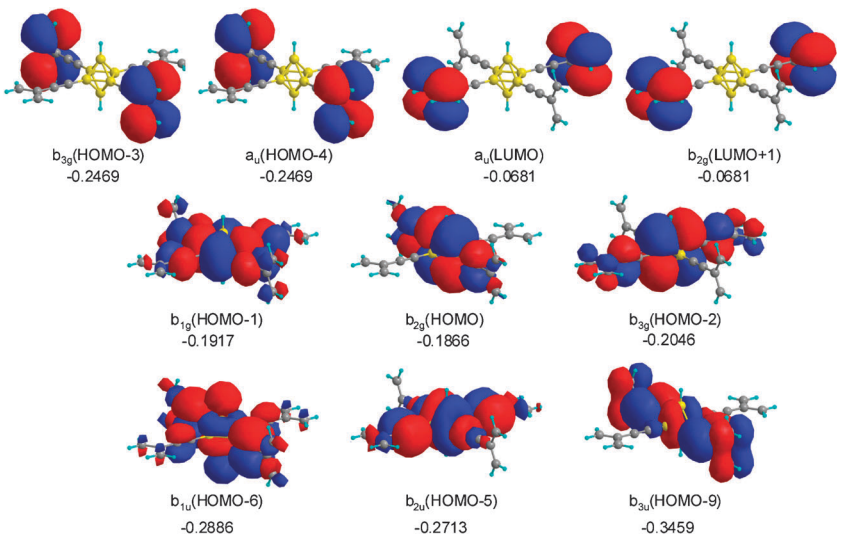

Fig. 9 Frontier molecular orbitals of molecule **2**, $B_6H_2(C{\equiv}CC_3H_4)_4$. Orbital energies are given in Hartree, obtained from ROHF calculations.

supermolecular system, where the allyl groups interact with $B_6H_6^{2-}$ *via* Van der Waals effects. The geometry optimizations of **3** and **4** converge onto equilibrium structures that correspond to the compressed octahedron, in which the boron–boron distance between the axial and the substituted equatorial boron is shortened compared to that between the axial and the unsubstituted equatorial boron (see Table 1). This can be explained by electrostatic attraction between borate dianion and allyl cations. Other geometrical parameters are very similar to those obtained from the hexa- and tetrasubstituted analogues.

The frontier molecular orbitals of **2**, **3**, and **4** are given in Fig. 9–11. When the substituent group is bonded to the borate cluster, molecular symmetry degrades from O_h to D_{2h}, and t_{2g} and t_{1u} evolve into B_g and B_u orbitals. The energy levels of $B_6H_6^{2-}$, **1**, **2**, **3**, and **4** are plotted in Fig. 12. For un-substituted $B_6H_6^{2-}$, the energy of the HOMO t_{2g} orbital is above 0, which shows that the un-substituted dianion is unstable in the gas phase and will spontaneously emit excess electrons. For molecule **1**, **2**, **3** and **4**, we can see that all B_g and B_u corresponding to t_{2g} and t_{1u} of $B_6H_6^{2-}$ are stable bonding orbitals, since the orbital energies are obviously lower than zero.

It is well established that there are two mechanisms to stabilize MCAs.[24] One is provided by the larger molecular space given by substituent ligands, because the large space allows the distribution of extra electrons, thus reducing their Coulomb repulsion. The other mechanism comes from the Coulomb attraction between MCAs and positively charged counterions. Molecule **1** demonstrates both mechanisms for stabilizing a borate cluster, because **1** has two electrophilic CN groups as well as the two mobile holes centered on allyl groups. Compared with **1**, **2** does not have CN groups, thus the energy of its frontier orbitals is higher than that of **1** because of the relatively smaller molecular space; but the anion-cation attraction is still sufficient to stabilize the boron cluster MCA. Molecules **3** and **4** show that the smaller molecular spaces are still able to contain extra charges, if the cation–anion interaction is present. **4** is totally substituent-free; however, due to the electrostatic interaction between allyl cations and the borate anion, the whole molecular system is still rather stable, which can be seen from the frontier molecular orbitals energies given in Fig. 12.

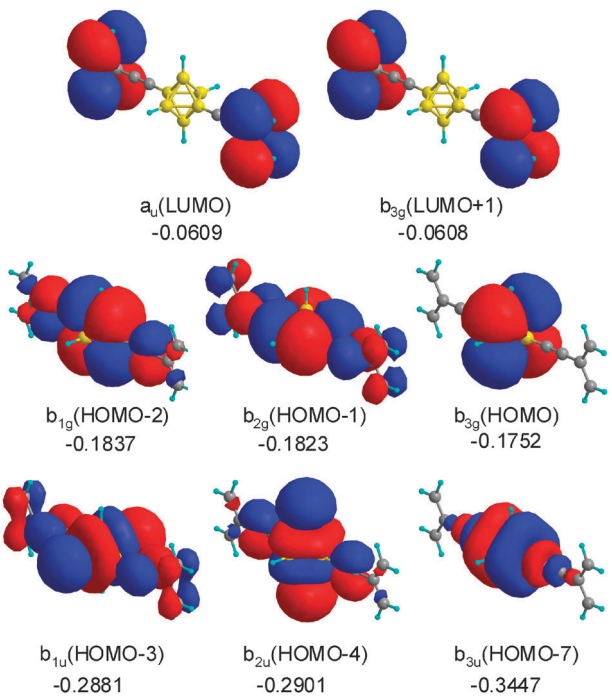

Fig. 10 Frontier molecular orbitals of molecule **3**, $B_6H_4(C{\equiv}CC_3H_4)_2$. Orbital energies are given in Hartree, obtained from ROHF calculations.

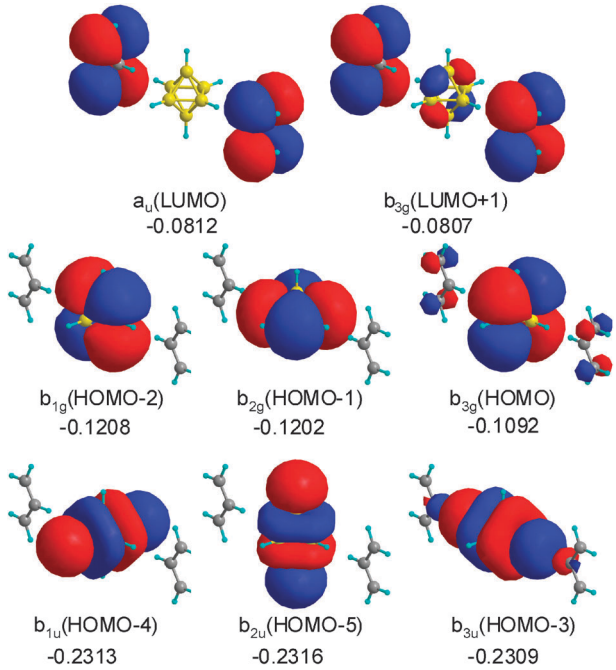

Fig. 11 Frontier molecular orbitals of molecule **4**, $B_6H_6(C_3H_5)_2$. Orbital energies are given in Hartree, obtained from ROHF calculations.

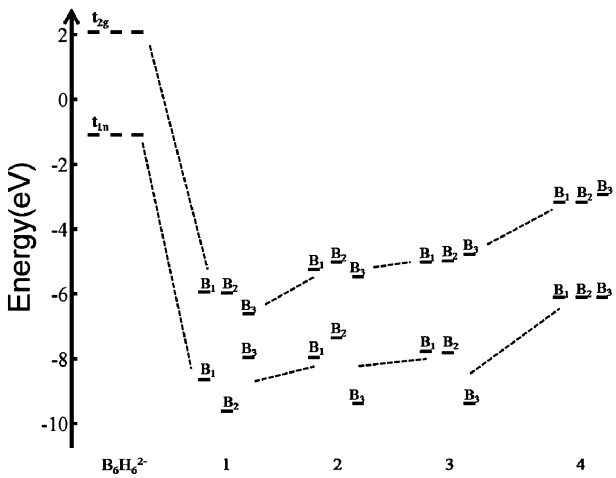

Fig. 12 Frontier molecular orbitals of $B_6H_6^{2-}$, $B_6(CN)_2(C{\equiv}CC_3H_4)_4$, $B_6H_2(C{\equiv}CC_3H_4)_4$, $B_6H_4(C{\equiv}CC_3H_4)_2$, and $B_6H_6(C_3H_5)_2$. Orbital energies are given in eV, obtained from ROHF calculations.

5. Summary

We explore the possibility of neutral QCA molecules, which include multiply charged anions MCAs,[23] specifically

closo-hexoborate dianion, as building blocks of candidate QCA molecules. Due to the charge-deficiency of this type of boron cluster, mobile charges are created in the molecular cell though the whole molecular cell remains charge neutral. This "self-doping" mechanism removes counterions from the QCA array, thus avoiding the complicated cation–anion pairing that may impede information processes. We demonstrate the "self-doping" of several model molecules. The switchability of molecule **1** was investigated using a molecular driver, which showed that mobile charges created by "self-doping" can be switched by a neighboring cell. Molecular orbital analysis suggests that electrostatic interaction between opposite charged moieties stabilizes the MCA building blocks. The above studies suggests stable, neutral, and switchable QCA molecules may indeed be possible.

The outlook for using boron clusters in the relevant synthesis chemistry is promising. For QCA applications, feasible working dots that can encode binary information may be provided by various metallocenes and their derivatives due to their chemical stability. In the past 20 years, zwitterionic metallocenes[41] have attracted considerable interest in the field of olefin polymerization catalysis since the pioneering work of Hlatky and Turner,[42] who serendipitously discovered a zwitterionic catalyst that includes a reactive zirconocene center covalently bound to an anionic triphenylborane. Interestingly, the motivation of investigating zwitterionic metallocene catalysts is to avoid the detrimental counterion effects—the same reason motivated us in this study of potential molecular electronic devices.

To date most studies of zwitterionic metallocene catalysts have been limited to systems containing a single boron atom,[43–46] although dianion boron clusters have been introduced in the chemistry of transition-metal zwitterions very recently.[47–50] Monoborane systems have a relatively small spatial volume and thus a weak ability to hold extra electrons. It is possible that many complexes thought to be zwitterionic are in fact stabilized by non-zwitterionic resonance or by partial hapticity.[51] Instead of the monoborane moiety, the larger *closo*-borate clusters suggested in this work are better charge containers because of the unique electronic structure of boron clusters.[39] For QCA implementation, this means that the mobile charges created in the working dots are well separated from the opposite charges, thus maintaining the binary characteristic of information encoded on the molecular charge configuration.

Our results may have a bearing on related issues in catalysis. For the implementation of zwitterionic metallocene catalysts, using a *closo*-borate cluster building block instead of a single boron atom may significantly increase the catalytic activity, since the metal center may demonstrate a stronger cationic characteristic. Also, due to the multiple charged anionic structures, more than one cationic metal centers can be built into the catalyst while the whole molecule still maintains charge neutrality. This may create a new type of zwitterionic catalyst with multiple reactive centers.

References

1 C. S. Lent, P. D. Tougaw, W. Porod and G. H. Bernstein, Quantum Cellular Automata, *Nanotechnology*, 1993, **4**, 49.
2 C. S. Lent and P. D. Tougaw, Lines of Interacting Quantum-Dot Cells: A Binary Wire, *J. Appl. Phys.*, 1993, **74**, 6227.
3 P. D. Tougaw and C. S. Lent, Logical Devices Implemented Using Quantum Cellular Automata, *J. Appl. Phys.*, 1994, **75**, 1818.
4 A. O. Orlov, I. Amlani, G. H. Bernstein, C. S. Lent and G. L. Snider, Realization of a Functional Cell for Quantum-Dot Cellular Automata, *Science*, 1997, **277**, 928.
5 M. Mitic, M. C. Cassidy, K. D. Petersson, R. P. Starrett, E. Gauja, R. Brenner, R. G. Clark and A. S. Dzurak, Demonstration of a silicon-based quantum cellular automata cell, *Appl. Phys. Lett.*, 2006, **89**, 013503.
6 F. Perez-Martinez, I. Farrer, D. Anderson, G. A. C. Jones, D. A. Ritchie, S. J. Chorley and C. G. Smith, Demonstration of a quantum cellular automata cell in a GaAs/AlGaAs heterostructure, *Appl. Phys. Lett.*, 2007, **91**, 032102.
7 K. K. Yadavalli, A. Orlov, J. P. Timler, C. S. Lent and G. L. Snider, Fanout gate in quantum-dot cellular automata, *Nanotechnology*, 2007, **18**, 375401.
8 I. Amlani, A. O. Orlov, G. Toth, G. H. Bernstein, C. S. Lent and G. L. Snider, Digital Logic Gate Using Quantum-Dot Cellular Automata, *Science*, 1999, **284**, 289.
9 H. Qi, S. Sharma, Z. Li, G. L. Snider, A. O. Orlov, C. S. Lent and T. P. Fehlner, Molecular quantum cellular automata cells. Electric field driven switching of a silicon surface bound array of vertically oriented two-dot molecular quantum cellular automata, *J. Am. Chem. Soc.*, 2003, **125**, 15250.
10 J. Jiao, G. J. Long, F. Grandjean, A. M. Beatty and T. P. Fehlner, Building Blocks of the Molecular Expression of Quantum Cellular Automata. Isolation and Characterization of a Covalently Bonded Square Array of Two Ferrocenium and Two Ferrocene Complexes, *J. Am. Chem. Soc.*, 2003, **125**, 7522.
11 J. Jiao, G. J. Long, L. Rebbouh, F. Grandjean, A. M. Beatty and T. P. Fehlner, Properties of a mixed-valence $(Fe^{II})_2(Fe^{III})_2$ square cell for utilization in the quantum cellular automata paradigm for molecular electronics, *J. Am. Chem. Soc.*, 2005, **127**, 17819.
12 H. Qi, A. Gupta, B. C. Noll, G. L. Snider, Y. Lu, C. S. Lent and T. P. Fehlner, Dependence of field switched ordered arrays of dinuclear mixed-valence complexes on the distance between the redox centers and the size of the counterions, *J. Am. Chem. Soc.*, 2005, **127**, 15218.
13 C. S. Lent, B. Isaksen and M. Lieberman, Molelar Quantum-Dot Cellular Automata, *J. Am. Chem. Soc.*, 2003, **125**, 1056.
14 Y. Lu and C. S. Lent, Theoretical study of molecular quantum-dot cellular automata, *J. Comput. Electron.*, 2005, **4**, 115.
15 Y. Lu, M. Liu and C. S. Lent, Molecular quantum-dot cellular automata: From molecular structure to circuit dynamics, *J. Appl. Phys.*, 2007, **102**, 034311.
16 Y. Lu and C. S. Lent, A metric for characterizing the bistability of quantum-dot cellular automata, *Nanotechnology*, 2008, **19**, 155703.
17 C. S. Lent, Bypass the Transistor, *Science*, 2000, **288**, 1597.
18 A. Bandyopadhyay, R. Pati, S. Sahu, F. Peper and D. Fujita, Massively parallel computing on an organic molecular layer, *Nat. Phys.*, 2010, **6**(5), 369.
19 Y. Lu, R. Quardokus, C. S. Lent, F. Justaud, C. Lapinte and S. A. Kandel, Charge localization in isolated mixed-valence complexes: an STM and theoretical study, *J. Am. Chem. Soc.*, 2010, **132**(38), 13519.
20 K. Walus and R. Budiman, Impurity charging in semiconductor quantum-dot cellular automata, *Nanotechnology*, 2005, **16**, 2525.
21 A. Dreuw, N. Zint and L. S. Cederbaum, Dianionic tetraborates do exist as stable entities, *J. Am. Chem. Soc.*, 2002, **124**, 10903.
22 N. Zint, A. Dreuw and L. S. Cederbaum, Gas-phase stability of derivatives of the *closo*-hexaborate dianion $B_6H_6^{2-}$, *J. Am. Chem. Soc.*, 2002, **124**, 4910.
23 A. Dreuw and L. S. Cederbaum, Multiply charged anions in the gas phase, *Chem. Rev.*, 2002, **102**(1), 181.
24 J. Kalcher and A. F. Sax, Gas phase stabilities of small anions: Theory and experiment in cooperation, *Chem. Rev.*, 1994, **94**, 2291.
25 S. N. Schauer, P. Williams and R. N. Compton, Production of small doubly charged negative carbon cluster ions by sputtering, *Phys. Rev. Lett.*, 1990, **65**(5), 625.
26 D. Schröder and H. Schwarz, Generation, stability, and reactivity of small, multiply charged ions in the gas phase, *J. Phys. Chem. A*, 1999, **103**, 7385.
27 G. R. Freeman and N. H. March, Chemistry of multiply charged negative molecular ions and clusters in the gas phase: terrestrial

and in intense galactic magnetic fields, *J. Phys. Chem.*, 1996, **100**(11), 4331.
28 C. S. Lent and B. Isaksen, Clocked molecular quantum-dot cellular automata, *IEEE Trans. Electron Devices*, 2003, **50**(9), 1890.
29 A. J. Cohen, P. Mori-Sánchez and W. Yang, Insights into current limitations of density functional theory, *Science*, 2008, **321**, 792.
30 R. H. Dederichs, S. Blugel, R. Zeller and H. Akai, Ground-states of constrained systems-application to gerium impurities, *Phys. Rev. Lett.*, 1984, **53**, 2512.
31 Q. Wu and T. Van Voorhis, Direct optimization method to study constrained systems within density-functional theory, *Phys. Rev. A*, 2005, **72**, 024502.
32 Q. Wu and T. Van Voorhis, Constrained density functional theory and its application in long-range electron transfer, *J. Chem. Theory Comput.*, 2006, **2**, 765.
33 Q. Wu and T. Van Voorhis, Direct calculation of electron tranfer parameters through constrained density functional theory, *J. Phys. Chem. A*, 2006, **110**, 9212.
34 P. Hohenberg and W. Kohn, Inhomogeneous electron gas, *Phys. Rev.*, 1964, **136**(3B), B864.
35 W. Kohn and L. J. Sham, Self-consistent equations including exchange and correlation effects, *Phys. Rev.*, 1965, **140**(4A), 1133.
36 H.-J. Werner, P. J. Knowles, F. R. Manby and M. Schütz, *MOLPRO, version 2010.1, a package of ab initio programs*, 2010.
37 T. P. Straatsma, E. Aprà, T. L. Windus, E. J. Bylaska, W. de Jong, S. Hirata, M. Valiev, M. Hackler, L. Pollack, R. Harrison, M. Dupuis, D. M. A. Smith, J. Nieplocha, V. Tipparaju, M. Krishnan, A. A. Auer, E. Brown, G. Cisneros, G. Fann, H. Früchtl, J. Garza, K. Hirao, R. Kendall, J. Nichols, K. Tsemekhman, K. Wolinski, J. Anchell, D. Bernholdt, P. Borowski, T. Clark, D. Clerc, H. Dachsel, M. Deegan, K. Dyall, D. Elwood, E. Glendening, M. Gutowski, A. Hess, J. Jaffe, B. Johnson, J. Ju, R. Kobayashi, R. Kutteh, Z. Lin, R. Littlefield, X. Long, B. Meng, T. Nakajima, S. Niu, M. Rosing, G. Sandrone, M. Stave, H. Taylor, G. Thomas, J. van Lenthe, A. Wong and Z. Zhang, *NWChem, a computational chemistry package for parallel computers, version 5.1.1 (2008)*, 2008.
38 A. Aviram, Molecules for memory, logic, and amplification, *J. Am. Chem. Soc.*, 1988, **110**, 5687.
39 K. Wade, Skeletal electron counting in cluster species-some generalizations and predictions, *Inorg. Nucl. Chem. Lett.*, 1972, **8**(559).
40 D. O. Cowan, P. Shu, F. L. Hedberg, M. Rossi and T. J. Kistenmacher, Ferricenyl(III)tris(ferrocenyl(II))borate. Synthesis, electrochemistry, and molecular structure of an unusual mixed-valence zwitterion, *J. Am. Chem. Soc.*, 1979, **101**(5), 1304.
41 W. E. Piers, Zwitterionic metallocenes, *Chem.–Eur. J.*, 1998, **4**(1), 13.
42 G. G. Hlatky, H. W. Turner and R. R. Eckman, Ionic, base-free zirconocene catalysts for ethylene polymerization, *J. Am. Chem. Soc.*, 1989, **111**, 2728.
43 E. F. van der Eide, W. E. Piers, P. E. Romero, M. Parvez and R. McDonald, Reaction of Bis(pentafluorophenyl)borane with methylidyne complexes: synthesis and characterization of a cationic tungsten(VI) borylalkylidyne hydride, *Organometallics*, 2004, **23**, 314.
44 L. W. M. Lee, W. E. Piers, M. Parvez, S. J. Rettig and V. G. J. Young, Zwitterionic metallocenes derived from rac and meso-ethylenebisindenyl zirconocene olefin complexes and pentafluorophenyl-substituted boranes, *Organometallics*, 1999, **18**, 3904.
45 K. S. Cook, W. E. Piers and R. McDonald, Synthesis and Chemistry of Zwitterionic Tantala-3-boratacyclopentenes: Olefin-like Reactivity of a Borataalkene Ligand, *J. Am. Chem. Soc.*, 2002, **124**, 5411.
46 B. E. Carpenter, W. E. Piers, M. Parvez, G. P. A. Yap and S. J. Rettig, Synthesis, characterization and chemistry of bis(pentafluorophenyl)boryl ferrocene, *Can. J. Chem.*, 2001, **79**, 857.
47 T. Marx, L. Wesemann and S. Dehnen, A zwitterionic transition-metal complex: platinum—closo-borate coordination synthesis, structure, and DFT calculations, *Organometallics*, 2000, **19**, 4653.
48 B. Ronig, I. Pantenburg and L. Wesemann, Zwitterionic molecules with stanna-closo-dodecaborate, *Z. Anorg. Allg. Chem.*, 2003, **629**, 1385.
49 B. Ronig, T. Bick, I. Pantenburg and L. Wesemann, Stannaborate chemistry: nucleophilic substitution at the cluster sphere, *Eur. J. Inorg. Chem.*, 2004, (4), 689.
50 L. Wesemann, Stanna-closo-dodecaborate: a new ligand in coordination chemistry, *Z. Anorg. Allg. Chem.*, 2004, **630**, 1349.
51 R. Chauvin, Zwitterionic organometallates, *Eur. J. Inorg. Chem.*, 2000, **4**, 577.

